Atmospheric Environment 288 (2022) 119300

Contents lists available at ScienceDirect

Atmospheric Environment

journal homepage: www.elsevier.com/locate/atmosenv

Imprints of anthropogenic air pollution sources on nitrate isotopes in precipitation in a tropical metropolitan area

Ricardo G. Passos [a], Ioannis Matiatos [b,*], Lucilena R. Monteiro [c], Rafael S.S.P. Almeida [a], Nilva P. Lopes [a], Carlos A. Carvalho Filho [a], Stela D.S. Cota [a]

[a] Centro de Desenvolvimento da Tecnologia Nuclear, CDTN - Campus UFMG, Av. Antônio Carlos 6627, CEP 31270-901, Belo Horizonte, MG, Brazil
[b] Hellenic Centre for Marine Research, Institute of Marine Biological Resources and Inland Waters, 46.7 km of Athens-Sounio Ave., 19013, Anavissos Attikis, Greece
[c] Instituto de Pesquisas Energéticas e Nucleares, IPEN/CNEN Av. Prof. Lineu Prestes, 2242, Cidade Universitária, CEP 05508-000, São Paulo, SP, Brazil

HIGHLIGHTS

- Urban and ship emissions were the main NO_x sources in precipitation NO_3^-.
- N emissions from wildfires in the Amazon area were identified in individual events.
- The period of lockdown in Belo Horizonte resulted in reduced vehicle emissions.
- High $\delta^{18}O$–NO_3^- in the cold period was partly due to formation via the N_2O_5 pathway.

GRAPHICAL ABSTRACT

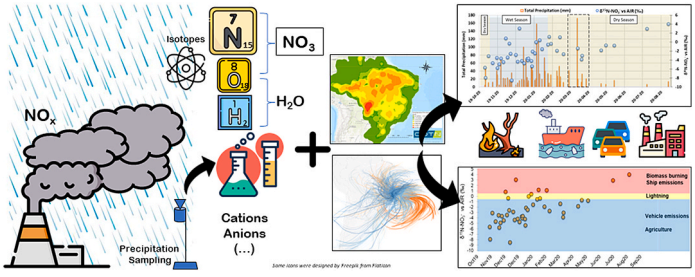

ARTICLE INFO

Keywords:
Stable isotopes
Wet deposition
Backward trajectory analysis
Geoprocessing
Tropics

ABSTRACT

Identifying the origin of NO_x emissions, their transformation into nitrate (NO_3^-) and its atmospheric deposition is important to better understand the impacts of air pollution on the environment and human health, on a local and regional scale. We measured nitrate isotopes ($\delta^{15}N$, $\delta^{18}O$ of NO_3^-) in precipitation samples in a tropical station in Brazil in 2019–2020 and combined them with chemical, geospatial and meteorological data to trace NO_x sources towards their wet deposition as NO_3^-. A total wet N deposition of ~12 kg N/ha.year showed significant N air pollution, out of which the relative contribution of NO_3^--N was ~37% (4.6 kg NO_3^--N/ha.year). The $\delta^{15}N$–NO_3^- values in precipitation ranged from −8.5 to +4.1‰, with a volume-weighted mean (VWM) value of −3.0 ± 2.7‰, whereas the $\delta^{18}O$–NO_3^- values ranged from +25.9 to +63.5‰ with a VWM value of +53.3 ± 7.3‰. The $\delta^{15}N$–NO_3^- results combined with air mass backward trajectory analysis and geospatial mapping revealed that the NO_x emissions in Belo Horizonte originated from: vehicles and industries from the urban and industrialized areas, biomass burning related to wildfires, and ship emissions from the coastal areas. The temporal variation of $\delta^{15}N$, $\delta^{18}O$ of NO_3^- values was attributed to NO_x source variability and transformation processes. The use of integrated methods to evaluate the imprints of anthropogenic air pollution sources in Brazil will contribute to inform NO_x source management strategies and improve air and water quality.

* Corresponding author.
E-mail address: i.matiatos@hcmr.gr (I. Matiatos).

https://doi.org/10.1016/j.atmosenv.2022.119300
Received 5 April 2022; Received in revised form 15 July 2022; Accepted 24 July 2022
Available online 31 July 2022

1. Introduction

The increasing energy, food and industrial production, and transport demand have elevated the levels of reactive nitrogen (N_r) species (e.g., nitrogen oxides (NO_x), and ammonia (NH_3)) in the atmosphere and consequently the amounts of N deposited to the aquatic environment, altering the N cycle (Galloway et al., 2004, 2008; Sutton et al., 2011; Villalobos-Forbes et al., 2021; Monteiro et al., 2021). Over the past thirty years, fossil fuel NO_x emissions, mainly from coal combustion and vehicle exhausts have accounted for about 95% of global NO_x emissions (Anenberg et al., 2017; Ohara et al., 2007). However, more recently Song et al. (2021) concluded that the non-fossil fuel NO_x can potentially account for about half of these emissions. Other possible sources such as soil biogenic processes, biomass burning, and lightning also contribute to the N_r species in the atmosphere (Fowler et al., 2013).

Once emitted to the atmosphere, NO_x is oxidized via several pathways to form highly soluble nitric acid ($HNO_{3(g)}$), which is then dissolved in precipitation or collected on aerosols, and subsequently scavenged from the atmosphere as wet deposition (Elliott et al., 2007). Excess nitrogen inputs can cause adverse effects on environmental quality, ecosystems, and human health. Nitrogen oxides are important drivers of atmospheric chemistry since they contribute to the formation of tropospheric ozone (O_3) and particulate matter in the air (Fang et al., 2011). Environmental damage includes haze, water, and soil acidification, plant biodiversity reduction, and eutrophication of streams, lakes, estuaries and the coastal zone (Bouwman et al., 2002, 2008; Stevens et al., 2004). NO_x emissions are also responsible for respiratory and cardiovascular diseases, such as cancer, asthma, bronchitis (Jiang et al., 2016), whereas high nitrate concentrations in drinking water can cause methemoglobinemia in infants (Comly, 1945; Donahoe, 1949). In the long-term, N air pollution and wet deposition can have detrimental effects on the economy (Sutton et al., 2011) and yield severe weathering of historical buildings and monuments (Sweevers and Van Grieken, 1992).

The stable isotopes of nitrate ($\delta^{15}N$, $\delta^{18}O$) have been widely used as tracers of the origin of NO_x emissions and the processes that N undergoes in the atmosphere and the terrestrial environment (Blarasin et al., 2020; Elliott et al., 2019; Felix and Murgulet, 2020; Jin et al., 2019; Li et al., 2019; Liu et al., 2017; Matiatos, 2016; Matiatos et al., 2021; Shi et al., 2021; Song et al., 2021; Villalobos-Forbes et al., 2021; Vystavna et al., 2020). The $\delta^{15}N$ of NO_3^- in precipitation generally "inherits" the $\delta^{15}N$ of NO_x source emissions assuming that N isotopic fractionation during the oxidation of NO_x is limited (Elliott et al., 2007; Freyer, 1991; Hastings et al., 2004; Heaton, 1990; Moore, 1977; Rose et al., 2019). Generally, the $\delta^{15}N$-NO_x from combustion power plant emissions show more positive values up to +26‰, whereas vehicle NO_x emissions show lower $\delta^{15}N$-NO_x values (−20 to +17‰) (Elliott et al., 2019 and references therein). Emissions from soil N emissions and fertilized areas show much lower $\delta^{15}N$-NO_x values (up to −60‰) (Elliott et al., 2019; Li and Wang, 2008). Nitrate isotope techniques can be more powerful when combined with other approaches such as atmospheric chemistry, satellite images, hydrometeorological assessment, mathematical modelling, and statistical tools (Bhuyan et al., 2020; Fu et al., 2019; Matiatos et al., 2022; Porfírio et al., 2020).

N and O isotope fractionation may occur due to photochemical transformations during transport, resulting in variable $\delta^{15}N$, $\delta^{18}O$ values in NO_3^- depending on the season and the meteorological conditions. For example, N isotope exchange between $NO_{(g)}$ and $NO_{2(g)}$ yields isotope fractionation resulting in ^{15}N enrichment in the oxidized form depending on ozone and sunlight conditions (Fang et al., 2011; Freyer et al., 1993; Matiatos et al., 2022). NO_2 further oxidizes to HNO_3(g) and triggers higher N isotope fractionation when oxidized through N_2O_5 formation and lower when oxidized through ·OH (Freyer, 1991; Morin et al., 2009; Walters et al., 2015). The oxidation through N_2O_5 formation also induces proportionally higher $\delta^{18}O$-NO_3^- values in winter due to higher contribution of tropospheric ozone (O_3) (+90 to +120‰, Krankowsky et al., 1995). The oxidation of NO_2 through ·OH is controlled by sunlight with lower O_3 contribution, hence lower $\delta^{18}O$-NO_3^- values are expected in summer. In general, $\delta^{15}N$–NO_3^- values are expected lower in summer and higher in winter, due to combined influence of possible source changes (e.g., more soil-derived biogenic emissions or lightning in summer *vs* more fossil fuel combustion - electricity generation in winter) and atmospheric oxidation processes (Elliott et al., 2019).

Air pollution is a major challenge in Brazil and responsible for more than 50,000 deaths per year (World Health Organization, 2017). NO_x emissions in Brazil are predominantly from fossil fuel burning from stationary sources like industrial plants or motor vehicles (César et al., 2015; de Miranda et al., 2012; Ferraz and Seroa da Motta, 2015; Macêdo and Ramos, 2020). NO_x emissions from vehicles in Brazil are more related to combustion of diesel fuel (42%) and less (25%) to gasoline (EPE, 2020). Diesel truck engines produce five times more NO_x than lighter gasoline-powered engines, per vehicle (Gaffney and Marley, 2009). According to Sant'Anna and Costa (2021), other major NO_x emissions in Brazil come from biomass (mostly firewood and charcoal) burning for cooking and heating at residencies (14 million families used biomass for cooking in 2018 and ~27% of residencies for energy, EPE, 2020). However, it is important to note that the demand for more heating during winter is limited in Brazil. NO_x emissions from fertilisers are also important in Brazil as being responsible for a significant share of the food produced in the world. In particular, Brazil was responsible for 22% of poultry meet, 15% of bovine meet, 17% of coffee, 13% of maize and 55% of soya beans global exports in 2018 (FAOSTAT, 2018). The biomes of the Amazon, Pantanal, and Cerrado regions, which represent vast ecosystems, have been severely affected by changes in the land-use and suffered from slash-and-burn practices. Lightning can also be a significant source of NO_x in subtropical and tropical regions (Schumann and Huntrieser, 2007).

In this study, we systematically measured the $\delta^{15}N$ and $\delta^{18}O$ of NO_3^- in precipitation in the city of Belo Horizonte, spanning rain events of one year (2019–2020) including the period of partial lockdown (20-03-20 to 20-04-20) enacted in the city due to the Covid-19 pandemic. Belo Horizonte is one of the most densely populated metropolitan regions in Brazil with ~2.5 million inhabitants in an area of 331 km^2 and diverse economic and industrial activities. We integrated nitrate isotope techniques with chemical, meteorological and spatial distribution information to assess the NO_x origin and related atmospheric oxidation processes and the N wet deposition in a tropical region of southeast Brazil. We also aimed to provide insight into the temporal evolution of atmospheric N dynamics and identification of seasonal patterns. This set of information is necessary for better understanding of how nitrogen pollutants in tropical urban environments are introduced in the terrestrial and aquatic environments via wet deposition and their potential impact and, therefore, inform for mitigation strategies to protect important ecosystems. To our knowledge this is the first systematic survey on nitrate isotopes in precipitation in Brazil.

2. Material and methods

2.1. Description of the study area

Our sampling station for rainwater was near the Nuclear Technology Development Center (CDTN/CNEN) in Belo Horizonte, within the campus of the Federal University of Minas Gerais (UFMG) (latitude −19.87°, longitude −43.97°, Elevation 848 m.a.s.l., Fig. 1a). The station was next to the CDTN meteorological station and surrounded by residencies and green areas. It was also located in the vicinity of a eutrophic lake (Lagoa da Pampulha), the regional airport, and the road network with high daily traffic flow during rush hours (Fig. 1b). An air pollution survey of 2015 showed that the NO_x emissions in Belo Horizonte and nearby cities originate mostly from motorways (86.1%) and industries (12.2%). The remaining 1.7% is attributed to biomass burning from residencies and other commercial activities (PETROBRAS, 2018). A lightning discharge density of 6/km^2/year was recorded in 2018 and

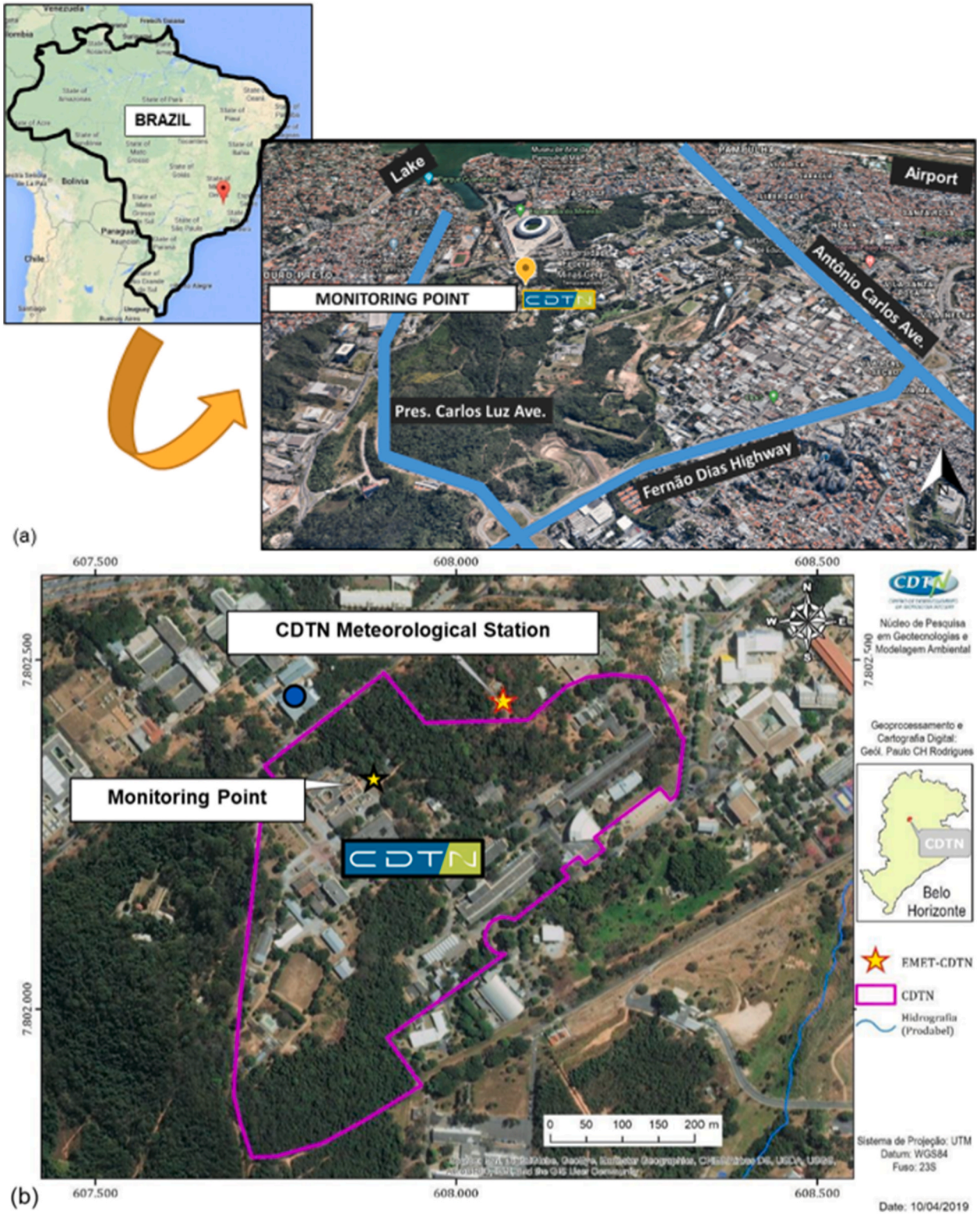

Fig. 1. Satellite images of the study area and the monitoring station: (a) Overview of the area and surroundings (Source: Google Earth®, 2020)); (b) CDTN area, highlighting by yellow stars the sampling station and the CDTN meteorological station (Source: Núcleo de Pesquisa em Geotecnologias e Modelagem Ambiental, CDTN). (For interpretation of the references to colour in this figure legend, the reader is referred to the Web version of this article.)

2019, with a total of ~2000 lightning occurrences/year. As one of the richest Brazilian regions in mineral resources, the Metropolitan Region of Belo Horizonte (RMBH) is responsible for 66% of the mining activity in the state of Minas Gerais, and the extraction of iron ore, manganese, gold, and limestone. The predominant industries in the region are steel, non-metallic minerals (cement and lime), petroleum, and the automobile industry (Gouveia et al., 2019).

2.2. Meteorological information and back trajectories

There are two well-defined seasons in Belo Horizonte due to the influence from mid latitude and tropical air masses (Lucio et al., 1999): dry/cold season (from April to October) and wet/warm (from November to March). In the dry season (winter), the area is predominantly influenced by the Atlantic Polar Front (APF), the South Atlantic Subtropical Anticyclone (SASA), and the Atlantic Polar anticyclone (through the Atlantic polar mass). In the wet season (summer) the convective systems associated with continental warming and the South Atlantic Convergence Zone (SACZ) prevail. High-pressure system (SASA) during the dry period inhibits the formation of rain clouds in Belo Horizonte and are responsible for the frequent occurrence of cloudless days, enhancing atmospheric pollution. Due to the warming of the South American continent, the high availability of moisture from the Amazon, and the frequent activity of the APF in the region, a significant increase in precipitation amount and RH in the rainy season is expected. Overall (according to last ten years of recorded data), the prevailing wind directions in the region are NE to SE; the mean annual wind speed and temperature is 2.6 m/s and ~22 °C (ranging between 9 °C and 34 °C), respectively. The mean annual atmospheric pressure is ~920 mbar, and the mean annual RH is ~60%, with lowest values in July, August, and September. Precipitation rates are typically >50 mm/h in the summer, and become moderate and lighter (<3 mm/h) in spring/autumn and in winter, respectively, with ~100 rainy days in total per year.

Meteorological information at our site was recorded using Campbell Scientific sensors fixed at a tower of 45 m height and included relative humidity (RH), air temperature, precipitation amount, solar radiation, wind speed and direction, and atmospheric pressure data at ground level, and at 10 and 40 m levels above ground from October 2019–September 2020. During this period, E to SE winds prevailed, with an average wind speed of 2.4 m/s (Fig. 2a). Higher temperatures (average value: 23.1 °C) and precipitation amount (total = 1,817.4 mm) were recorded in the wet season (November–March) compared to the dry season (average temperature of 21.1 °C and precipitation amount of 216.4 mm) although surprisingly high temperatures were recorded in September and October (average value for these months = 24.5 °C) (Fig. 2b). The highest volumes of daily precipitation (>100 mm/d) were recorded in January, much higher than the yearly average in the region (Fig. 2c). Rain events had a duration of ~3–4 days, starting with low intensity rain that gradually increased and decreased during the last day.

To investigate the transport of NO_x from long distances and its effect on precipitation, the timings of the rain events were isolated from the meteorological data and the hybrid Single-particle Lagrangian Integrated Trajectory Model (HYSPLIT) was used to calculate air masses backward trajectories of each sampling day, on a 92-h basis and 1-h timestep, at initial altitudes of 500, 700, 900, 1000, 1500, 2500, 4000 m. Each trajectory was calculated using NOAA's meteorological data files. The ending altitude of air masses was set to the mean elevation of the CDTN (~850 m above sea level). The trajectories were coupled with precipitation monitoring parameters (ions and isotopes) and geospatial maps.

2.3. Sampling methodology

Event-based precipitation sampling was carried out over the period from October 2019 to September 2020 (number of event samples (n) = 57; 12 in the dry season and 45 in the wet season). The samples were collected systematically at 10 a.m. with a bulk collector, provided the sample volume was ≥100 mL, following the WMO guidelines (WMO, 2004). The monitoring period overlapped the period of partial lockdown (20 March - April 20, 2020) in the city of Belo Horizonte due to the Covid-19 pandemic.

A small aliquot of each sample was used to determine the temperature (T, in °C), the dissolved oxygen (DO, in mg/L), the redox potential (ORP, in mV), pH (−) and the electrical conductivity (EC, in μS/cm). A glass electrode probe DM-2P (Digimed®) was used for pH, ORP, and T readings; IntelliCAL LDO101 (HACH®), luminescent/optical digital

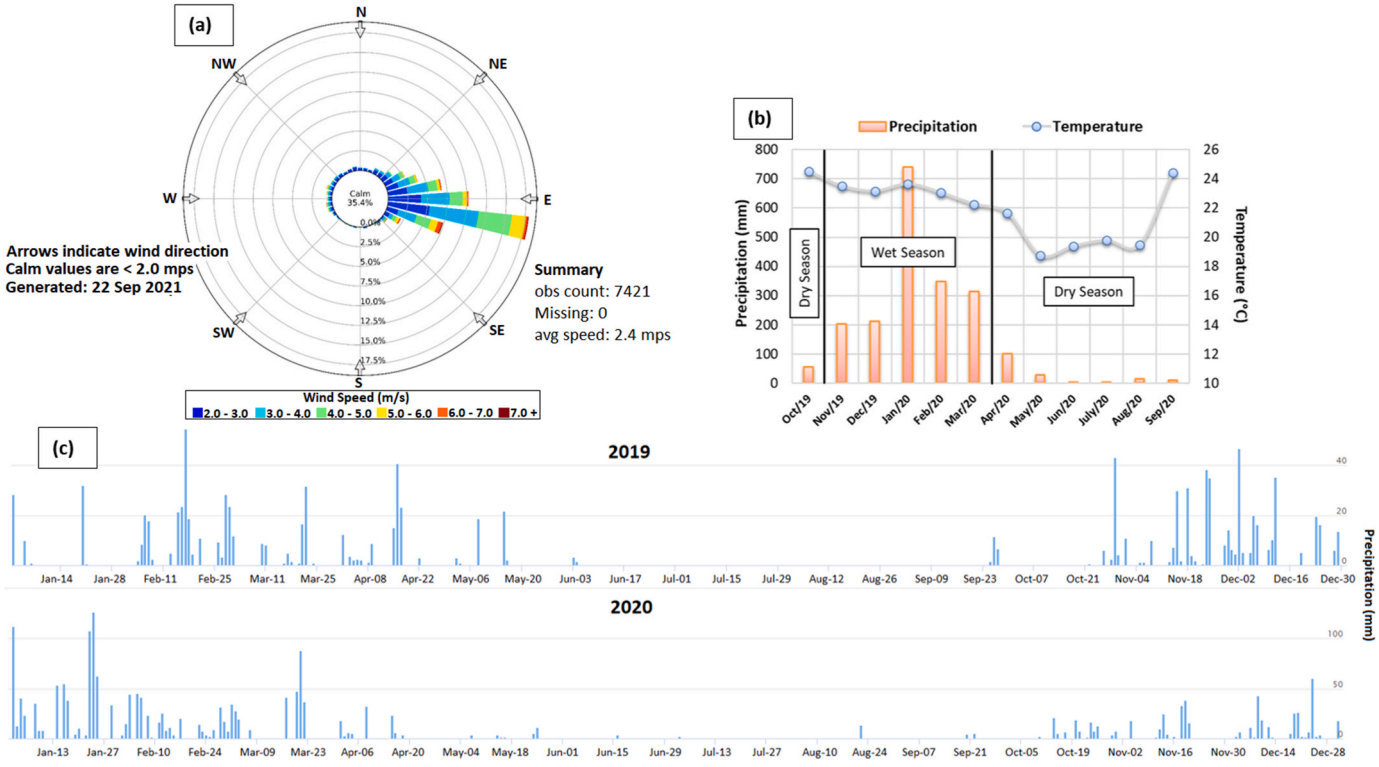

Fig. 2. (a) Wind speed, frequency and direction, and (b) average temperature and total precipitation by month, for the specific monitoring period of this study (October 2019 to September 2020); (c) Graphical summary with daily precipitation data recorded throughout 2019 and 2020 by the National Institute of Meteorology (INMET).

probe was used for DO readings, and IntelliCAL CDC401 4-Poles Graphite Conductivity Cell probe for EC readings (HACH®). Samples of 50–100 mL were stored in pre-cleaned HDPE bottles at dark and frozen conditions (−20 °C), until they were dispatched for isotopic analysis. Unacidified and acidified (with HNO_3^- until the pH was equal 2) samples of 30 mL were stored in precleaned HDPE bottles at dark and in cool conditions (4 °C) until they were analysed for anions and cations, respectively. All samples were previously filtered using 0.45 μm polytetrafluorethylene (PTFE) syringe membranes.

2.4. Laboratory analysis techniques

Major cations and anions in precipitation samples were determined at the Chromatography Laboratory in CDTN using Ion Exchange Chromatography (CTI) system (Shimadzu) equipped with degasser (DGU-20As), pump (LC-10ADvp), automatic injector (SIL-20A), oven (CTO-20A), conductivity detector (CDD-6A) and controller (SCL-10Avp). For anion analysis, a Shim-Pack IC-A1 column (100 × 4.6 mm) and a Shim-Pack IC-GA1 (10 × 4.6 mm) pre-column (both Shimadzu) were used. For cation analysis, a Shim-Pack IC-C1 column (150 × 5.0 mm) and a Shim-Pack IC-GC1 (10 × 4.0 mm) pre-column (both Shimadzu) were used. Quantification was performed by external standardization, using multi-point calibration. The tests were carried out in triplicate. The detection limits (DL) for individual elements were estimated as 0.1 mg/L for anions and 0.05 mg/L for cations. To evaluate the reliability of the chemical analysis results we applied the principle of electroneutrality of water according to the acceptance criteria proposed by (APHA, 2005) (Fig. S1, in Supplementary Material).

For nitrate isotopes (^{15}N and ^{18}O of NO_3^-) the samples were analysed at the Isotope Hydrology Laboratory by using the Ti(III) reduction method, which involves a one-step chemical conversion of NO_3^- to N_2O gas in septum sample vials (Altabet et al., 2019). The N_2O headspace was measured for $^{15}N/^{14}N$ and $^{18}O/^{16}O$ ratios by coupling with a continuous-flow isotope-ratio mass spectrometer (IRMS) and a trace gas N_2O purification device. The stable isotope ratios were expressed in delta (δ) and per mil (‰) notation relative to an international standard (reference):

$$\delta(‰) = \left[\left(\frac{R_{sample}}{R_{reference}}\right) - 1\right] x1000 \quad \text{(Equation 01)}$$

where R_{sample} and $R_{reference}$ are the ratio of the heavy-to-light isotope in a sample and the international reference, respectively). Regarding the nitrate isotopes, $R = {}^{15}N/{}^{14}N$ was used for nitrogen, and $R = {}^{18}O/{}^{16}O$ for oxygen. Atmospheric N_2 was the isotopic reference for nitrogen, and the Vienna Standard Mean Ocean Water (VSMOW) for oxygen. The analytical uncertainties were ±0.2‰ and ±0.4‰ for $\delta^{15}N$ and $\delta^{18}O$–NO_3^-, respectively. The standards used for nitrate isotope analysis were USGS34 (−1.8 ± 0.1 for $\delta^{15}N_{AIR}$ and +27.9 ± 0.3‰ for $\delta^{18}O_{VSMOW\text{-}SLAP}$), USGS35 (+2.7 ± 0.1‰ for $\delta^{15}N_{AIR}$ and +57.5 ± 0.3‰ for $\delta^{18}O_{VSMOW\text{-}SLAP}$), and IAEA-$NO_3$ (+4.7 ± 0.2‰ for $\delta^{15}N$ AIR and +25.6 ± 0.4‰ for $\delta^{18}O_{VSMOW\text{-}SLAP}$).

2.5. Data processing

The volume-weighted mean concentrations (VWM) of the rainwater constituents were calculated to eliminate the influence of different rainfall intensities. The VWM, which takes into account the effect of dilution by the rainfall amount (Bhuyan et al., 2020), was expressed in mg/L or μmol/L and was calculated as follows:

$$VWM = \frac{\sum_{i=1}^{n} C_i P_i}{\sum_{i=1}^{n} P_i}. \quad \text{(Equation 02)}$$

where C_i is the ionic concentration of each ion (in mg/L or μmol/L) and P_i is the volume of each rainy event (mL or mm). In addition, the wet deposition (WD, in kg/ha) of the species to a specified period was also calculated (Equation (03)):

$$WD\ (kg/ha) = \frac{VWM\ \left(\frac{mg}{L}\right) \times P\ (mm)}{100} \quad \text{(Equation 03)}$$

where P is the total of the precipitation in the period considered (mm).

Prior data processing, the raw data were tested for normality (Shapiro-Wilk test), before applying hypothesis tests to compare sample groups from different periods (e.g., wet and dry). Student's t-test and the Mann-Whitney *U* test were applied to determine whether the differences between the mean and the median values of different groups were significant. A *p*-value of 0.05 was used as a threshold of significance. The Shapiro-Wilk test showed that no variable follows the normal distribution but $\delta^{15}N$–NO_3^-. Therefore, for statistical comparison between differences in the seasonal periods considering the average values, the Student's t-test was used for the $\delta^{15}N$–NO_3^- data and the Mann-Whitney *U* test for all other variables.

To explore the possible influence of isotopic fractionation in the oxidation processes, we estimated the equilibrium isotope fractionation of nitrogen isotopes of NO to NO_2 (f_{NO2}) using the method of Li et al. (2019) based on the NO_2/O_3 ratios. In brief, the f_{NO2} triggers a shift in $\delta^{15}N$–$NO_{2(shift)}$ relative to $\delta^{15}N$-NO_x in the atmosphere. The NO_2/O_3 ratios for Belo Horizonte by month were obtained from FEAM - Fundação Estadual de Meio Ambiente de Minas Gerais (2022). The isotope fractionation between NO and NO_2 in the atmosphere during NO_x photochemical cycling is considered one of the most significant ones (Freyer et al., 1993). Other isotope fractionation processes, such as NO_2 to NO_3^-, remain unclear in a realistic, field-based environment, with controversial isotope effects (Liu et al., 2020) and thus they were not considered.

Spearman's correlation tests (for non-parametric data), Pearson's correlation, and simple linear regression analysis (for parametric data) were applied to investigate correlations between variables. Cluster analysis was performed in the trajectories twice to identify similar origins: one based on the trajectory's spatial distribution that considered the latitude and longitude with the objective of grouping the trajectories according to their geographical origins and a second one based on nitrate isotopes ($\delta^{15}N$ and $\delta^{18}O$) with the objective of grouping the trajectories according to their isotopic signatures. The Calinski-Harabasz criterion was used to assess cluster quality (Karna and Gibert, 2022). Statistica 8.0® software was used to perform the statistical analyses.

2.6. Geospatial mapping of pollution sources

Regional geospatial maps of potential sources of NO_x were produced in a Geographic Information System (GIS) environment. Thematic maps of lightning, roads occupation, forest/agricultural fires, livestock, industries, and sewage treatment plants were performed using the non-parametric Kernel Density tool with smoothing option, which calculates the density of occurrences of the theme by an area value (Fieberg, 2007). The roads occupation map was elaborated by a weighting calculus between the relevance of the road and the size of the city that this road was passing through. Ports information was obtained in a georeferenced base available only in point feature, which was used to locate the ports in the map. The relative importance of each port for emissions, considered from the size, activity, and official classification, was represented on the map by the size and colour of the point. The maps were elaborated using the GIS-based software ESRI ArcGIS Pro® with public georeferenced bases, most of them provided by the Brazilian Government through the INDE (National Spatial Data Infrastructure) platform. Table S1 of Supplementary Material summarizes the weights that were used in the Kernel Density calculation.

3. Results

3.1. Chemical characteristics and N wet deposition

Around 98% of the rain water samples showed a VWM pH value above the reference value of 5.6 (pH value of cloud water at equilibrium with atmospheric CO_2, Charlson and Rodhe, 1982) (Table 1) indicating that rainwater was neutral to alkaline. The order of the VWM molar concentrations, from the higher to the lower, was $K^+ > NH_4^+ > Ca^{2+} > Na^+ > Mg^{2+}$ for cations, and $Cl^- > NO_3^- > SO_4^{2-} > F^- > NO_2^- > PO_4^{3-}$ for anions (Table 1). The VWM values of the molar concentrations, showed that: i) rainwater acidity is almost totally neutralized ($H^+/(NO_3^- + SO_4^{2-}) = 0.02$); ii) the relative contribution of NO_3^- and Cl to rainwater acidity via HNO_3^- and HCl was predominant compared to SO_4^{2-} ($NO_3^- + Cl^-)/SO_4^{2-} = 9.49$); iii) most of the N was in its reduced form [$NH_4^+/NO_3^- = 1.57$]; iv) there was a significant alkaline influence in precipitation [$(Ca^{2+}+NH_4^+)/(NO_3^- + SO_4^{2-}) = 2.21 > 1$].

The VWM NO_3^- concentration values in rainwater were 15.5 μmol/L (mean = 18.6 μmol/L), or 1.0 mg/L (mean = 1.2 mg/L). Based on the VWM (mg/L), the total wet deposition flux of NO_3^- was 20.5 kg NO_3^-/ha.year, and the total N deposition (sum of NO_2^--N, NO_3^--N and NH_4^+-N) was 12.4 kg N/ha.year, with a relative nitrate contribution of ~37% (4.6 kg NO_3^--N/ha.year) (Table 1).

3.2. Stable isotope results

The $\delta^{15}N$–NO_3^- values in precipitation ranged from −8.5 to +4.1‰, with a VWM value of −3.0 ± 2.7‰ (mean value = −2.4‰, Table 1, Fig. 3). Most $\delta^{15}N$–NO_3^- values were between −5.2‰ and +1.1‰, with more than 75% being negative ($P_{75\%} = -0.6$‰) (Fig. 4a) and concentrated in the expected range for NO_x emissions from fossil fuel burning, biomass burning, and lightning, (Fig. 4b). The values of $\delta^{15}N$–NO_3^- were plotted within the expected ranges for near-road environments and gasoline-powered vehicles (tailpipe) (Fig. 4b) rather than diesel-powered vehicles. The $\delta^{18}O$–NO_3^- values in precipitation ranged between +25.9 and +63.5‰, with a VWM value of +53.3 ± 7.3‰ (Table 1), falling within the expected precipitation ranges (Kendall et al., 2008). The NO_2/O_3 ratios at Belo Horizonte ranged from 0.35 in October to 0.88 in June, which produced a $\delta^{15}N$–$NO_{2(shift)}$ relative to $\delta^{15}N$-NO_x of +2.4 to +4.9‰, respectively (Table S2 of Supplementary Material).

3.3. Temporal variations and correlations

There was significant difference (*p-value*< 0.05) between wet and dry season for NO_3^-, NO_2^-, SO_4^{2-}, Mg^{2+} and Ca^{2+} with highest values in the dry season but not all other variables. However, a decreasing trend for NO_3^- and $\delta^{18}O$-NO_3^- values was identified in the wet season with lowest peaks in February–March (Fig. 5a). On the contrary, an increasing trend was revealed for $\delta^{15}N$-NO_3^- in the wet season till March, which increased further in the dry season after slightly declining in April during the lockdown period (Fig. 5b). The NH_4^+/NO_3^- molar ratio values ranged between 0.0 and 7.5 with highest peaks in the wet season, reaching a value of ~8 (Fig. 6c). High peaks of NH_4^+/NO_3^- and NH_4^+ (4.0 and 2.7, respectively) lower than those of December 2020 (7.5 and 7.0, respectively) were identified during the lockdown period (Fig. 6a, b, 6c), together with lowering of the $\delta^{15}N$-NO_3^- values (Fig. 6d). No significant change was recorded for $\delta^{18}O$-NO_3^- during the same period (Fig. 6e).

Almost all ion variables showed a significant negative correlation with precipitation. The strongest correlation value obtained ($r = 0.78$) was between Ca^{2+} and Mg^{2+}. A significant and strong correlation was identified between SO_4^{-2} and NO_3^- ($r = 0.72$). The $\delta^{15}N$–NO_3^- values showed no significant correlation with any of the parameters, except a negative correlation with air (r = −0.35) and rainwater temperature ($r = -0.42$, Table S3 of Supplementary Material) (i.e., higher $\delta^{15}N$–NO_3^- in colder period).

3.4. Sources maps and back trajectories

Most of the NO_x sources showed a higher density in the south-eastern area of the country, corresponding to the states of Rio de Janeiro and São Paulo, and in the metropolitan regions of the country (around state capitals), with the highest population density, number of industries and traffic (Fig. 7a and b). The port map exhibited higher density along the

Table 1
- Average concentrations/deposition (volume-weighted mean - VWM, mean, and median – Med.), minimum (Min.), maximum (Max.), and standard deviation (SD) values of the water quality parameters measured in situ and laboratory (anions and cations), as well as the observed isotopic ratios – entire monitoring period.

In situ	n[a]	VWM	Mean	Med.	Min.	Max.	SD	
pH (−)	57	6.4	6.8	6.8	5.5	7.9	0.5	
Temperature (°C)	57	24.6	24.9	24.9	20.8	28.8	1.7	
EC (μS/cm)	56	16.8	21.8	16.5	2.3	87.9	16.8	
DO (mg/L)	55	7.4	7.4	7.4	6.6	8.3	0.4	
ORP (mV)	49	272.6	281.1	286.0	176.4	453.9	56.4	
Isotopes								
$\delta^{15}N - NO_3^-$ (‰)	43	−3.0	−2.4	−2.8	−8.5	4.1	2.7	
$\delta^{18}O - NO_3^-$ (‰)	43	53.1	53.1	54.5	25.9	63.5	7.3	
Anions								**WD (kg/ha.yr)[b]**
F^- (μmol/L)	44	2.4	3.2	0.7	0.2	62.6	10.7	3.8
Cl^- (μmol/L)	50	31.6	45.2	43.3	2.5	163.6	36.0	24.7
NO_2^- (μmol/L)	35	1.9	2.0	1.9	1.6	3.6	0.4	1.8[b]/0.6[c]
NO_3^- (μmol/L)	56	15.5	18.6	14.8	1.5	52.3	12.6	20.5[b]/4.6[c]
SO_4^{2-} (μmol/L)	55	5.0	6.9	4.7	0.2	32.3	7.7	105
PO_4^{3-} (μmol/L)	5	1.6	1.8	1.3	0.6	4.5	1.5	3.0
Cations								
Mg^{+2} (μmol/L)	32	5.3	7.0	4.9	0.6	31.3	7.1	2.6
Ca^{+2} (μmol/L)	57	20.8	31.9	18.7	7.4	222.8	38.3	17.0
Na^+ (μmol/L)	42	15.4	20.5	8.9	3.0	160.5	29.7	7.4
NH_4^+ (μmol/L)	46	24.3	29.4	26.8	0.6	71.5	18.8	9.3[b]/7.2[c]
K^+ (μmol/L)	46	31.3	41.2	35.7	0.7	138.1	32.5	25.1

[a] n = number of valid data (not censored values).
[b] WD considering species concentrations in mg/L.
[c] WD expressed as N for NO_3^-, NO_2^- and NH_4^+. OBS.: Br^- values were all below the detection limit and so they are not presented.

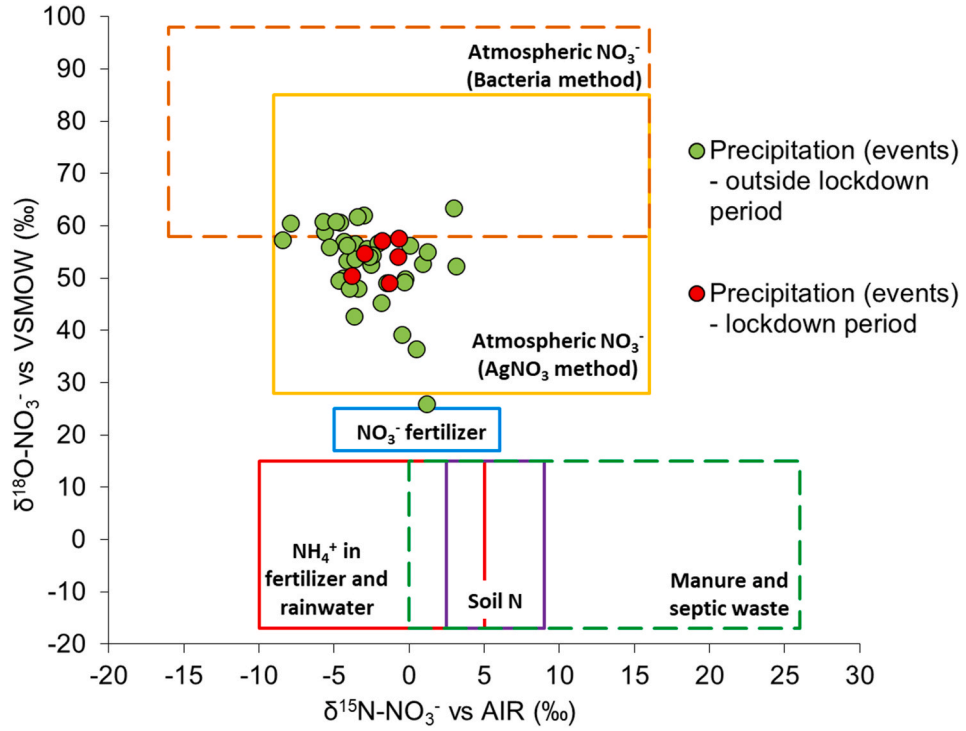

Fig. 3. Dual isotope diagram of $\delta^{15}N$ and $\delta^{18}O$ of NO_3^- (Kendall et al., 2008).

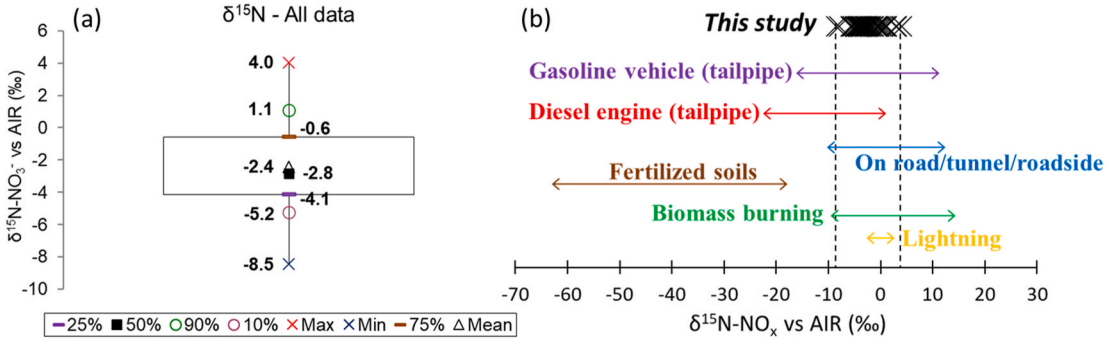

Fig. 4. $\delta^{15}N$–NO_3^- in precipitation data: (a) Box-plot graph from all monitoring data; (b) Monitoring values in this study *vs* literature values by emission sources (ranges are from Elliott et al., 2019 and references therein).

coast and particularly of the southeast region (Fig. 7f). In turn, emissions from livestock activity, sewage treatment plants and lightning hot spots showed higher density in the southern part of the country (Fig. 7c, e, 7g). Biomass burning hot spots were identified mostly in the Pantanal, Amazon and Cerrado regions (Fig. 7d).

The clustering analysis of trajectories (Fig. 8a) based on latitude and longitude information resulted in 3 clusters that reflect differences in geographical origin, which mainly differ in distance covered and origin/direction of air masses (Fig. 8b). The green cluster (G1) included air masses trajectories from the South, which passed through regions of significant air pollution from vehicles, industries, agriculture, and livestock, and presented low $\delta^{15}N$–NO_3^- values (mean = −3.7‰). The red cluster (R1) included trajectories from the East, which passed through regions of intense ship traffic and port activity and marine influence. This cluster showed high NO_3^- concentrations and $\delta^{15}N$–NO_3^- values (mean = −0.8‰) compared to the other clusters. The blue cluster (B1) represented trajectories that originated from the central regions of the country, including large areas of agriculture (mean $\delta^{15}N$–NO_3^- = −2.1‰).

The clustering analysis based on $\delta^{15}N$–NO_3^- and $\delta^{18}O$–NO_3^- data resulted in 5 different clusters of trajectories (Fig. 8c): i) the green cluster (G2) with very positive $\delta^{15}N$–NO_3^- values (mean = +3.7‰) and high NO_3^- concentrations (mean = 0.5 mg/l as NO_3^--N) originating from the ocean and crossing the Brazilian coast; ii) the light blue cluster (LB2) with positive $\delta^{15}N$–NO_3^- values (mean = +0.4‰) originating from the ocean and crossing the Brazilian coast but away from the ports; iii) the red (R2) and orange (O2) clusters with negative $\delta^{15}N$–NO_3^- values coming from the northwest part of the country (mean $\delta^{15}N$–NO_3^- of −3.1‰ and −4.9‰, respectively); and iv) the dark blue cluster (DB2) representing more local trajectories, with slightly negative $\delta^{15}N$–NO_3^- values (mean = −0.5‰).

The maximum values of K^+ and F^-, i.e., 138.1 μmol/L and 62.6 μmol/L respectively, were found in trajectories originating from the Pantanal region (Fig. 8d). Considerably high Na^+ values, 113.1 and 160.5 μmol/L (as reference, 90% percentile ($P_{90\%}$) = 35.5 μmol/L), were found in the two precipitation events that occurred during the period 26–30 December 2019, and corresponding to long-range oceanic air masses from south-eastern Argentina (Fig. 8e). Trajectories presenting $\delta^{15}N$–NO_3^- values around zero showed variable origins (Fig. 8f).

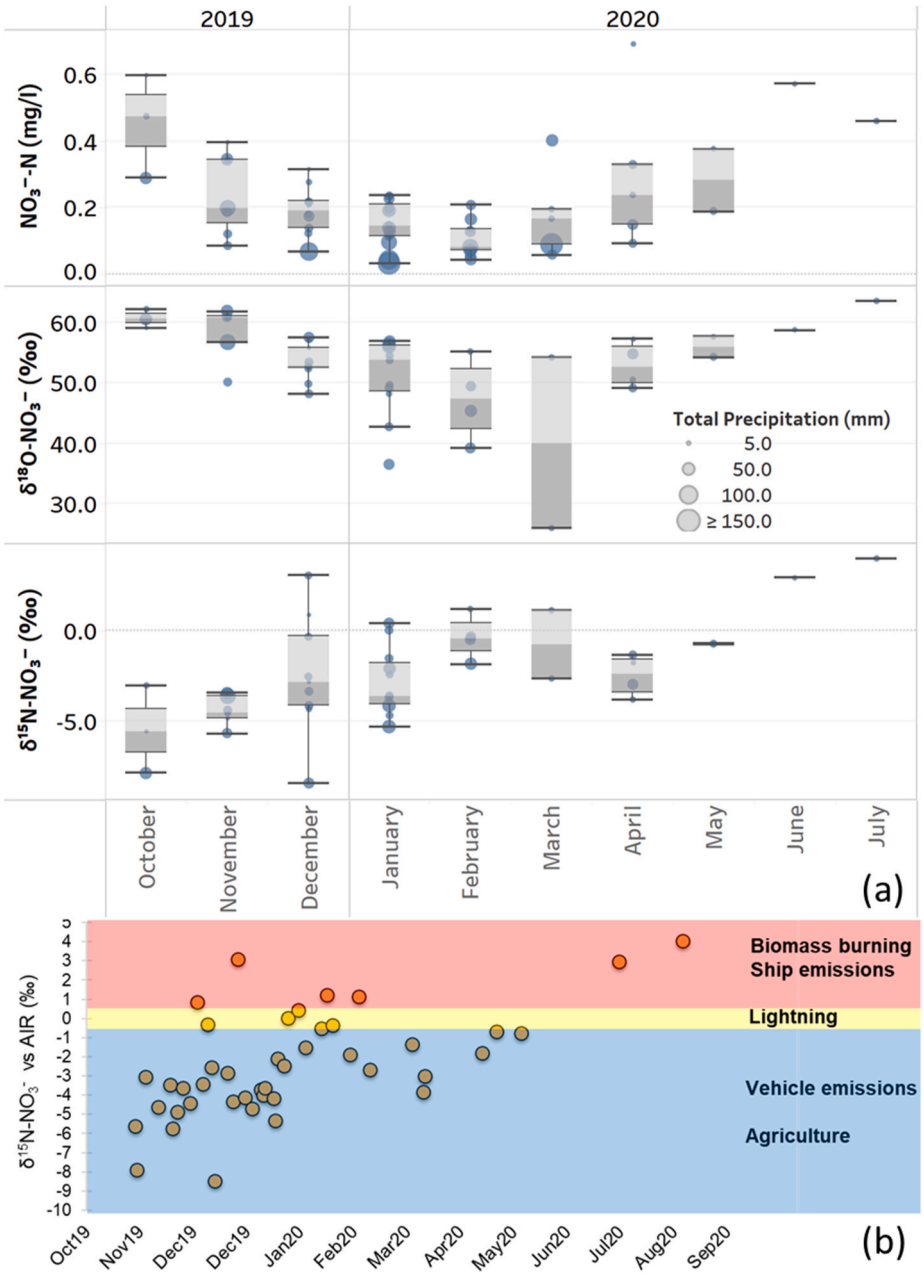

Fig. 5. (a) Precipitation data and Box-plot graphs of the N–NO_3^- concentration (mg/L), $\delta^{18}O$–NO_3^- vs SMOW (‰), and $\delta^{15}N$–NO_3^- vs AIR (‰) during the monitoring period (from top to bottom); (b) Values along the monitoring period classified according to three isotopic signature classes based on the expected sources of NO_x, air masses backward trajectories, monitoring data and literature consultation in this paper.

4. Discussion

4.1. N deposition

The VWM NO_3^- concentration values in rainwater were similar to those reported in a tropical site in Costa Rica (mean = 22.2 μmol/L, Villalobos-Forbes et al., 2021) or to those reported in the Metropolitan Region of Rio de Janeiro (Brazil) (VWM = 15.8 μmol/L, De Mello, 2001), ~350 km away from our monitoring site. However, our values were lower than those reported for densely populated cities in India and China (Jin et al., 2019; Liu et al., 2017; Shi et al., 2021), but significantly higher than those observed in undisturbed remote areas (2.5 μmol/L), including central Amazonia (Andreae et al., 1990; Galloway et al., 1982). Our reported NO_3^- values classified the study area at an intermediate level in terms of air pollution namely between clean and heavily polluted atmospheric environments.

The total N deposition in the region (12.4 kg N/ha.year) was in the range of 2–20 kg/ha.year reported by (Vet et al., 2014) as low-level deposition in densely populated and/or intensively cultivated areas. Our value was lower than those reported in other urban areas in China (26.8 kg N/ha.year (Zhao et al., 2009) or >30 kg N/ha.year (Liu et al., 2006; Zhang et al., 2008)). Given that N deposition values > 53 kg N/ha.year have been considered as indicators of serious N pollution (Jia and Chen, 2010; Souza et al., 2006), the average value in the current work can be considered as indicative of an intermediate-to-low polluted area in terms of N. The total N deposition exceeded the critical load of 5–10 kg N/ha.year for N deposition impacts in natural or semi-natural ecosystems and oligotrophic waters (Bobbink et al., 2010; Unece, 2004).

The average wet deposition flux of NO_3^- (20.5 kg NO_3^-/ha.year) was within the range of values reported for northern Brazil (12.8–28.0 kg

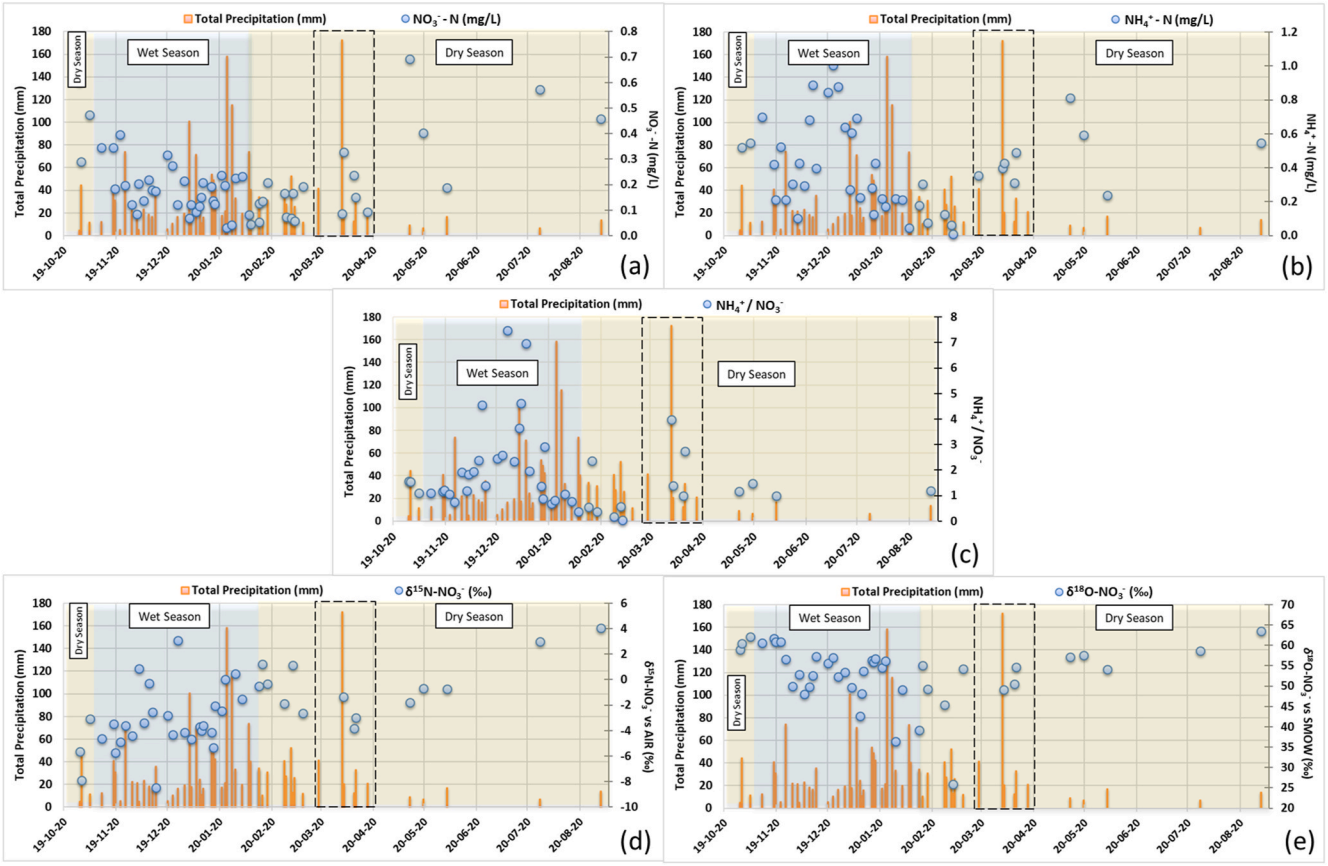

Fig. 6. Time-series plots for the monitoring period showing precipitation data (orange bars) and (a) NO_3^- concentration; (b) NH_4^+ concentration; (c) NH_4^+/NO_3^- molar ratio; (d) $\delta^{15}N$–NO_3^-; and (e) $\delta^{18}O$–NO_3^- (blue dots). Shaded colours highlight the seasonal period and the dashed rectangles highlight the period of a partial lockdown in the city due to the COVID-19 pandemic. (For interpretation of the references to colour in this figure legend, the reader is referred to the Web version of this article.)

NO_3^-/ha.year, Porfírio et al., 2020), Canada (0.4–26.5 kg NO_3^-/ha.year, Cheng and Zhang, 2017) and Costa Rica (20.5 kg NO_3^-/ha.year, Villalobos-Forbes et al., 2021). However, they were higher than those reported for China (16.0 and 18.5 kg NO_3^-/ha.year, Fang et al., 2011) and much higher than the overall annual deposition (7.73 kg NO_3^-/ha.year) in Germany (Beyn et al., 2014).

4.2. Assessment of nitrogen origins

4.2.1. Chemical indicators

The high values of Cl^-, Ca^{2+}, and K^+, and their correlations were attributed to emissions from sea salts (ocean air masses), industries, and biomass burning (De Mello, 2001; Yu et al., 2018). The high values of Ca^{2+} can be attributed to dust, crust, or to emissions from the cement and iron/steel industries and limestone soil abundant in the area (Anatolaki and Tsitouridou, 2009; Banerjee, 2008; Kim et al., 2003; Samara et al., 1992) (Fig. S2 of Supplementary Material). The strong correlation between SO_4^{-2} and NO_3^- revealed their common origin and similar chemical process, which could be due to burning of fossil fuels, industrial processes, and combustion of biomass (Hoinaski et al., 2014). The correlation between NO_3^- and NH_4^+ suggested that these two compounds in wet deposition may be due to agricultural and livestock activities. Vegetation can be the dominant source of K- and Ca-containing aerosols in the Atlantic Forest region in south-eastern Brazil.

The NH_4^+/NO_3^- molar ratio in wet deposition has been linked to the degree of industrialization (Zhao et al., 2009). For example, NH_4^+/NO_3^- molar ratios $\ll 1$ have been recorded in highly industrialized areas (e.g., North America) whereas those >1 in areas with intensive agriculture, such as in the Midwestern USA, parts of Europe, and in rural China (Fahey et al., 1999; Xie et al., 2008; Zhang et al., 2008; Zhao et al., 2009). In this study, the high NH_4^+/NO_3^- molar ratios (>1) could be due to influence from distal and local agricultural areas and activities. This could also be the reason for the ~60% higher contribution of NH_4^+-N to the total N deposition (7.2 kg N– NH_4^+/ha.year) compared to NO_3^--N deposition (4.6 kg N– NO_3^-/ha.year).

The "peak" region of NH_4^+/NO_3^- molar ratio was observed in the middle of the wet and warm season (till January), when the NH_4^+/NO_3^- molar ratios were close to 8 (Fig. 6c), with three samples having NH_4^+/NO_3^- values higher than 90% percentile ($P_{90\%} = 3.8$). This can be explained by higher NH_4^+ concentrations due to more agricultural influence compared to vehicle/industries emissions (NO_x), given that the period of nitrogen fertilization of crops and pastures in the region occurs predominantly from October to January. This was also confirmed by the backward trajectory analysis that showed air masses originating predominantly from the agricultural region of the country, without passing through the urbanized southeast areas. The reduced NH_4^+/NO_3^- values from January till March (before the lockdown period and after the nitrogen fertilization period) indicated the predominance of contribution from vehicle emissions over agricultural emissions (Passos et al., 2021). In turn, high NH_4^+/NO_3^- values observed in the period of the partial lockdown can be explained by the decrease in vehicle circulation and industrial activities in the city (Passos et al., 2021), which allowed the influence from fertilized and natural soils becoming more evident.

4.2.2. Isotopic indicators

The wide range of $\delta^{15}N$–NO_3^- values indicated that there are multiple sources of NO_x (i.e., vehicle and ship emissions, biomass burning and lightning) that contribute in nitrate deposition in Belo Horizonte. On average, our $\delta^{15}N$–NO_3^- values (-3.0 ± 2.7‰) were much lower than those reported for Costa Rica ($+0.7 \pm 2.2$‰, Villalobos-Forbes et al.,

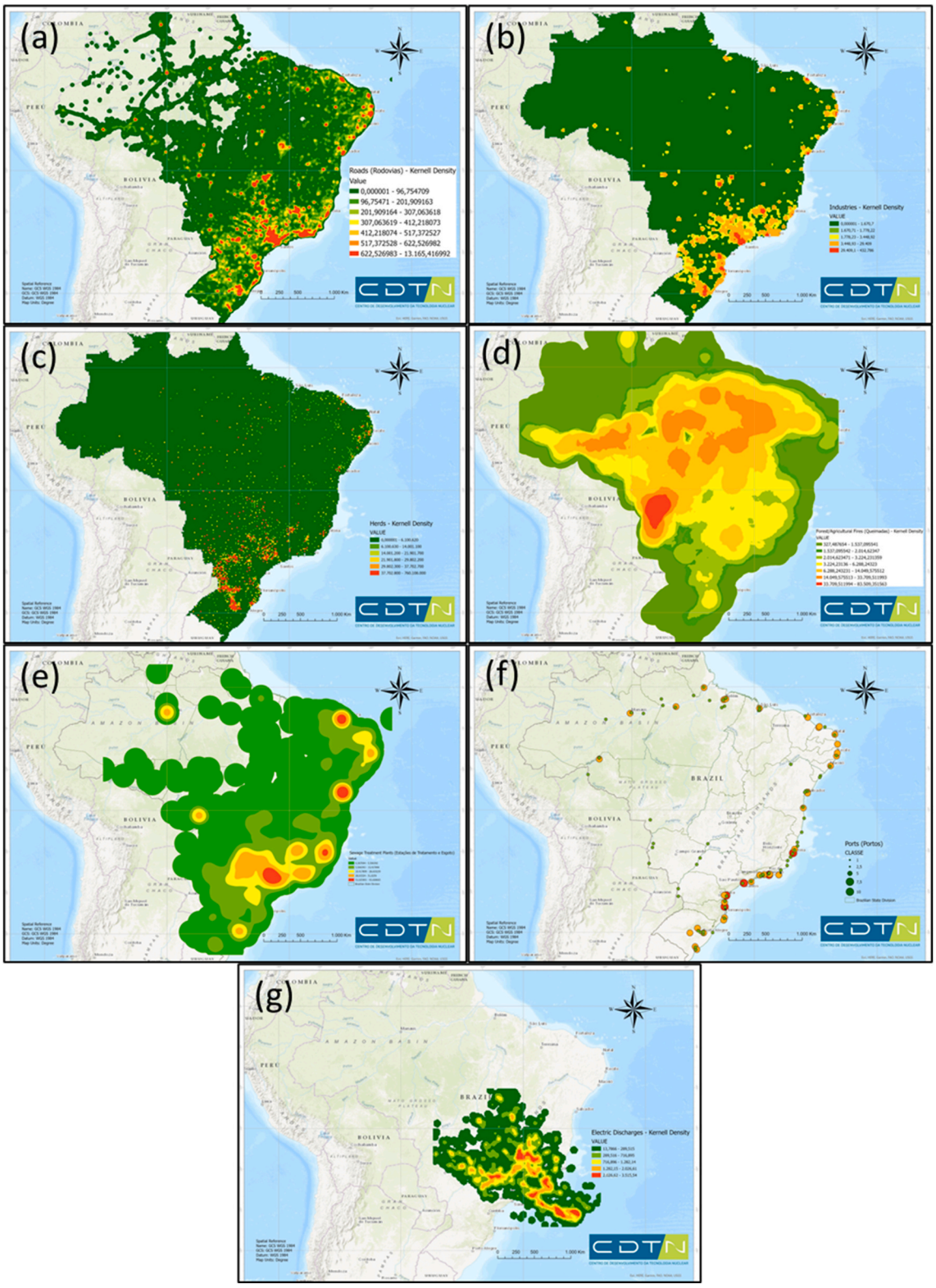

Fig. 7. Kernel density maps of reactive nitrogen sources: (a) roads occupation (traffic); (b) industries; (c) livestock; (d) biomass burning; (e) sewage treatment plants (f) ports; (g) lightning (missing data for the northwest region).

2021), other urban areas in Europe (+0.8 ± 2.6‰, Song et al., 2021), the Midwestern and north-eastern United States (−1.5‰, Elliott et al., 2007), and areas of East Asia influenced by coal combustion emissions, indicating enhanced contribution from fertilized and agricultural areas. The lack of significant difference in $\delta^{15}N–NO_3^-$ values between the wet and the dry season were attributed to the overall influence of the same NO_x emissions sources throughout the year. The shift of $\delta^{15}N–NO_3^-$ to lower values during the lockdown period could be due to enhanced influence from fertilized soils and reduced influence from the vehicle emissions, but still it is not possible to claim the dominance of the first over the latter. Moreover, the low $\delta^{15}N–NO_{2(shift)}$ values (+2.8‰, on average) relative to mixed $\delta^{15}N\text{-}NO_x$ in the atmosphere during the wet

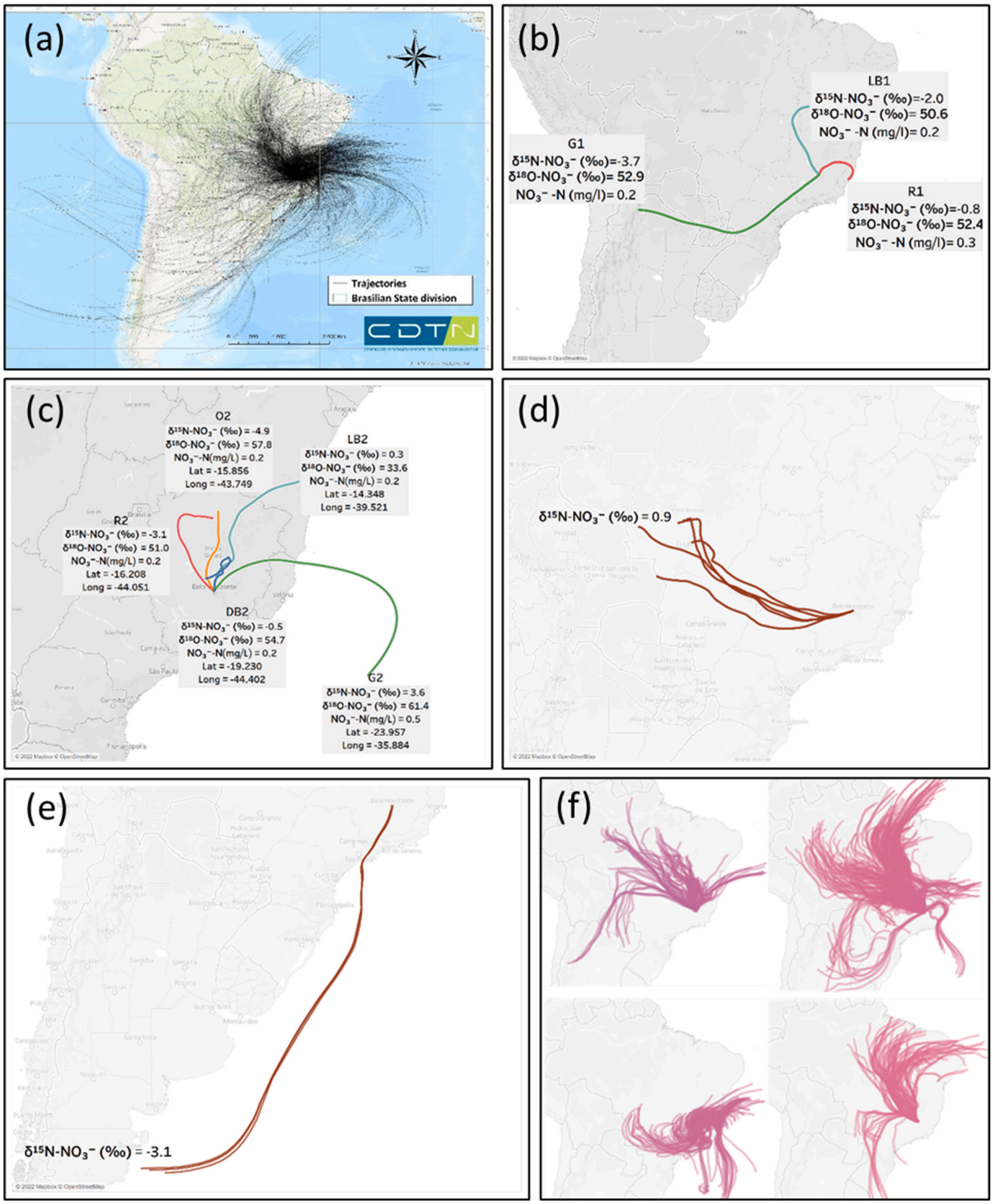

Fig. 8. 96-h air masses backward trajectories for the sampling period October 2019–September 2020: (a) All trajectories (N = 2536); (b) Clusters based on latitude and longitude data with average values of NO_3^- concentration (mg/L), $\delta^{15}N–NO_3^-$ vs AIR (‰) and $\delta^{18}O–NO_3^-$ vs SMOW (‰) (c) Clusters based on $\delta^{15}N–NO_3^-$ and $\delta^{18}O–NO_3^-$ with average Latitude and Longitude; (d) Trajectories with maximum values of K^+ and F^- in Pantanal region; (e) Coastal trajectories with highest Na^+ values; (f) Trajectories with $\delta^{15}N–NO_3^-$ values around zero (−0.5 to +0.5‰).

(warm) season, including the lockdown period of March and April (+3.1‰, on average), could also be masking the influence from the sources; however, the relatively low shift in this period induced the least bias to NO_x source values.

The negative correlation of $\delta^{15}N–NO_3^-$ with air and rainwater temperature ($r = -0.42$) (i.e., higher $\delta^{15}N–NO_3^-$ in colder times), corresponds to different atmospheric oxidation processes for the formation of NO_3^-. The isotope exchange equilibrium between $NO_{(g)}/NO_{2(g)}$ and NO_3^- is temperature-dependent and typically results in more enriched ^{15}N in colder times (Elliott et al., 2007; Xing and Liu, 2012). This was also confirmed by the highest NO_2/O_3 values that were recorded in June (dry season), which induced the highest $\delta^{15}N–NO_{2(shift)}$ relative to mixed $\delta^{15}N\text{-}NO_x$ in the atmosphere (+4.9‰). However, in Bermuda and Israel, $\delta^{15}N–NO_3^-$ was significantly higher in the warmer season (Hastings et al., 2003; Wankel et al., 2010). Despite the correlation with temperature in this study, a clear pattern of seasonal $\delta^{15}N–NO_3^-$ differences (wet/hot vs dry/cold) was not detected.

The negative values of $\delta^{15}N–NO_3^-$ (mean = −3.7‰) of the green cluster (G1) of trajectories originating from the southern highly populated regions, such as the Metropolitan Region of Sao Paulo (MRSP), were attributed to increased emissions from vehicles. The MRSP is responsible for 65% of the total NO_x emissions in the country (CETESB, 2020). The less negative $\delta^{15}N–NO_3^-$ values (mean = −0.8‰) of the red cluster of trajectories (R1) originating from the East could be attributed to emissions from ships due to intense ship traffic and port activity at the coast. According to Beyn et al. (2015), the $\delta^{15}N–NO_3^-$ ranges of ship traffic are poorly investigated, but the kind of combustion process, the engine technology, and the use of heavy oil causes higher $\delta^{15}N$ values of NO_x. An increasing trend of NO_x emissions from ships has led to higher NO_x loads derived from ships in the last decades (Matthias et al., 2010). The formation of nitrate-bearing aerosol particles induced by sea salt and the impact of ship emissions both on aerosol formation and as a NO_x emission source caused surprisingly high $\delta^{15}N–NO_3^-$ and NO_3^- values corresponding to the red cluster (R1). Ship emissions lead to higher isotope values at coastal sites and higher NO_3^- loads (Beyn et al., 2015; Shi et al., 2021; Zhang et al., 2016; Zong et al., 2020). Lightning ($\delta^{15}N–NO_3^- \sim 0$‰), as a possible source of NO_x, can be linked to the R1 cluster of trajectories given its passing through regions with extreme lightning occurrence (Fig. 7h). The blue cluster of trajectories (B1) passes through large areas of agriculture and livestock activity that could explain the negative $\delta^{15}N–NO_3^-$values, which was also confirmed by the source maps (Fig. 7c).

The $\delta^{15}N–NO_3^-$ values of the green cluster of trajectories (G2) (mean = +3.7‰) originating from the ocean and across the Brazilian coast could be attributed to ship emissions. The $\delta^{15}N–NO_3^-$ values of the light blue cluster (LB2) of trajectories (mean = +0.5‰) coming from the ocean but far from the ports could be indicative of influence from lightning hotspots. The negative $\delta^{15}N–NO_3^-$ values of the red (R2) and orange (O2) clusters of trajectories coming from agricultural regions in the northwest of the country (mean of −3.1‰ and −4.9‰, respectively) were attributed to emissions from agricultural activity (e.g., sugar cane, soybeans). The dark blue cluster (DB2) of trajectories (mean $\delta^{15}N–NO_3^-$ = −0.5‰) was influenced by emissions from local vehicles and industries and possibly lightning, due to its short range. In addition, three out of eight trajectories that form the dark blue cluster had a concentration of Ca^{+2} higher than the 90% percentile of all data ($P_{90\%} = 75.8$ μmol/L), which is possibly related to the local cement industries and mining activities, supporting the higher local influence hypothesis compared to the other trajectories.

The maximum values of K^+ and F^- were recorded from 29 November to December 2, 2019 for those trajectories coming from the Pantanal wetlands (Fig. 8d), which suffered from wildfires during the monitoring period together with greater Amazon area. Both ions are indicative of biomass burning (Ando et al., 2001; Tiwari et al., 2012), which was confirmed by a $\delta^{15}N–NO_3^-$ value of +0.9‰ recorded in the precipitation one day after their outbreak. Biomass burning hot spots due to wildfires in those areas were also confirmed by the source maps (Fig. 7d).

The two precipitation events that occurred during the period 26–30 December 2019 showed an average $\delta^{15}N–NO_3^-$ value of +3.1‰ and the highest Na^+ values. Given that the air masses of these events originated from the Brazilian coast in the south, this was attributed to the influence from ship emissions along the coast. In general, averaged $\delta^{15}N–NO_3^-$ values were lower for precipitation from the continent than from the ocean, are also reported by Fang et al. (2011).

All $\delta^{15}N–NO_3^-$ values around zero (−0.5 to +0.5‰) were observed in the period between December and February, which concentrates the highest occurrence of lightning. The corresponding backward trajectories showed that air masses indeed originated from lightning hotspots (Fig. 8f). In Brazil lightning plays an important role, as the country has the highest lightning incidence in the world, with about 70 million every year (Junior and Pinto, 2021).

4.3. Atmospheric processes related to N deposition

The overall low $\delta^{18}O$ of NO_3^- values can be partly linked to the dominance of the hydroxyl radical (•OH) pathway of atmospheric NO_3^- over dinitrogen pentoxide (N_2O_5) pathway in the tropics (Alexander et al., 2009). Solar radiation and higher sunshine hours during the hot/wet season favour the influence of the oxidation processes with •OH and lower the $\delta^{18}O–NO_3^-$ values. In turn, the N_2O_5 pathway can be more relevant in the cold season due to the low intense solar radiation and fewer sunshine hours, explaining slightly higher $\delta^{18}O–NO_3^-$ values. However, despite the seasonal variation of $\delta^{18}O–NO_3^-$ (Fig. 5), the difference between the two periods (+57.4‰ and +53.7‰) was not statistically significant, suggesting that the atmospheric conditions in the monitoring region was not the only responsible for these values. Cold season temperatures can induce higher ^{15}N in N oxidized species (e.g., HNO_3) (Calvert et al., 1985; Freyer et al., 1993; Morin et al., 2008), as explained earlier, but the absence of a similar trend for $\delta^{18}O–NO_3^-$ could be due to dominance of source isotope signature over isotope fractionation (Fang et al., 2011; Elliott et al., 2019; Felix and Murgulet, 2020). The low $\delta^{18}O–NO_3^-$ in the wet season can also be attributed to precipitation amount effect and isotope fractionation. Heavy isotopes are preferentially incorporated into the condensed phase and then rapidly washed out during the long-distance transport of nitrogen-containing particles, resulting in the depletion of ^{18}O (and ^{15}N) in precipitation NO_3^- (Shi et al., 2021).

5. Conclusions

We presented a systematic monitoring of nitrate isotopes in precipitation in a tropical site in Brazil and coupled it with chemical, geospatial modelling, and meteorological data to better understand the origin and dynamics of atmospheric nitrate and N deposition. The total N deposition load showed intermediate-to-low air pollution, which can contribute in the degradation of sensitive ecosystems. Chemical, isotope, geospatial and back trajectory analysis data revealed two major origins of NO_3^- air pollution: i) urban emissions (incl. vehicles and industries), local and long-range transported from the densely populated southern regions and ii) ship emissions from the ocean and the coastal zone. Other trajectories clusters showed influence from agricultural activities/livestock from the northern part of the country, and possible lightning influence locally. Individual rain events demonstrated influence by N combustion emissions from wildfires that occurred in the Amazon area during the monitoring period. The period of lockdown in Belo Horizonte resulted in reduced vehicle emissions, which was reflected in the chemical and isotope indicators, increasing the influence from soil and agricultural N emissions. Although no significant differences in isotope and chemical values were recorded, an increasing trend towards the dry/cold period was identified, which was attributed to fewer sunshine hours and higher contribution of the N_2O_5 pathway in the formation of precipitation NO_3^-. The knowledge of NO_x sources and the dynamics

involved in their wet deposition as NO_3^- will contribute to more targeted and effective measures to mitigate NO_x emissions in Brazil to improve air quality and reduce the environmental, economic, and public health impacts.

CRediT authorship contribution statement

Ricardo G. Passos: conceived the study, performed the monitoring and data interpretation, and wrote the manuscript. **Ioannis Matiatos:** performed data interpretation and wrote the manuscript. **Lucilena R. Monteiro:** performed data compilation and revised the manuscript. **Rafael S.S.P. Almeida:** performed GIS analysis. **Nilva P. Lopes:** performed laboratory analysis and revised the manuscript. **Carlos A. Carvalho Filho:** performed data interpretation and revised the manuscript. **Stela D.S. Cota:** performed data interpretation and revised the manuscript.

Declaration of competing interest

The authors declare that they have no known competing financial interests or personal relationships that could have appeared to influence the work reported in this paper.

Data availability

Data will be made available on request.

Acknowledgements

This research was partly funded and analytically supported by the International Atomic Energy Agency, IAEA's Coordinated Research Project F32008 entitled "Global Monitoring of Nitrogen Isotopes in Atmospheric Waters". The authors gratefully acknowledge the NOAA Air Resources Laboratory (ARL) for the provision of the HYSPLIT transport and dispersion model and READY website (https://www.ready.noaa.gov) used in this publication. We thank S. Terzer-Wassmuth for his contribution on HYSPLIT trajectories processing. Thanks to C. Douence for conducting nitrate isotope measurements. We also thank the anonymous reviewers for their insightful comments and suggestions that helped improving the manuscript.

Appendix A. Supplementary data

Supplementary data to this article can be found online at https://doi.org/10.1016/j.atmosenv.2022.119300.

References

Alexander, B., Hastings, M.G., Allman, D.J., Dachs, J., Thornton, J.A., Kunasek, S.A., 2009. Quantifying atmospheric nitrate formation pathways based on a global model of the oxygen isotopic composition (Δ17O) of atmospheric nitrate. Atmos. Chem. Phys. 9 (14), 5043–5056.

Altabet, M.A., Wassenaar, L.I., Douence, C., Roy, R., 2019. A Ti (III) reduction method for one-step conversion of seawater and freshwater nitrate into N2O for stable isotopic analysis of 15N/14N, 18O/16O and 17O/16O. Rapid Commun. Mass Spectrom. 33 (15), 1227–1239.

American Public Health Association, 2005. APHA Standard Methods for the Examination of Water and Wastewater. Standard Methods for the Examination of Water & Wastewater. American Public Health Association, Washington, DC.

Anatolaki, C., Tsitouridou, R., 2009. Relationship between acidity and ionic composition of wet precipitation: a two years study at an urban site, Thessaloniki, Greece. Atmos. Res. 92, 100–113.

Ando, M., Tadano, M., Yamamoto, S., Tamura, K., Asanuma, S., Watanabe, T., Kondo, T., Sakurai, S., Ji, R., Liang, C., Chen, X., 2001. Health effects of fluoride pollution caused by coal burning. Sci. Total Environ. 271 (1–3), 107–116.

Andreae, M.O., Talbot, R.W., Berresheim, H., Beecher, K.M., 1990. Precipitation chemistry in central Amazonia. J. Geophys. Res. Atmos. 95 (D10), 16987–16999.

Anenberg, S.C., Miller, J., Minjares, R., Du, L., Henze, D.K., Lacey, F., Malley, C.S., Emberson, L., Franco, V., Klimont, Z., Heyes, C., 2017. Impacts and mitigation of excess diesel-related NOx emissions in 11 major vehicle markets. Nature 545 (7655), 467–471.

Banerjee, D., 2008. Study of precipitation chemistry over an industrial city. Int. J. Environ. Sci. Technol. 5, 331–338.

Beyn, F., Matthias, V., Dähnke, K., 2014. Changes in atmospheric nitrate deposition in Germany–an isotopic perspective. Environ. pollut. 194, 1–10.

Beyn, F., Matthias, V., Aulinger, A., Dähnke, K., 2015. Do N-isotopes in atmospheric nitrate deposition reflect air pollution levels? Atmos. Environ. 107, 281–288.

Bhuyan, P., Ahmed, M.S., Hopke, P.K., Hoque, R.R., 2020. Understanding the chemistry and sources of precipitation ions in the mid-Brahmaputra valley of northeastern India. Aerosol Air Qual. Res. 20 (12), 2690–2704.

Blarasin, M., Cabrera, A., Matiatos, I., Lutri, V., Maldonado, L., Giacobone, D., Matteoda, E., Becher Quinodoz, F., Giuliano Albo, J., Eric, C., Felizzia, J., 2020. Application of isotope techniques to enhance the conceptual hydrogeological model and to assess groundwater sustainability in the Pampean plain in Córdoba, Argentina. Isot. Environ. Health Stud. 56 (5–6), 402–417.

Bobbink, R., Hicks, K., Galloway, J., Spranger, T., Alkemade, R., Ashmore, M., Bustamante, M., Cinderby, S., Davidson, E., Dentener, F., Emmett, B., 2010. Global assessment of nitrogen deposition effects on terrestrial plant diversity: a synthesis. Ecol. Appl. 20 (1), 30–59.

Bouwman, A.F., Van Vuuren, D.P., Derwent, R.G., Posch, M., 2002. A global analysis of acidification and eutrophication of terrestrial ecosystems. Water Air Soil Pollut. 141 (1), 349–382.

Calvert, J.G., Lazrus, A., Kok, G.L., Heikes, B.G., Walega, J.G., Lind, J., Cantrell, C.A., 1985. Chemical mechanisms of acid generation in the troposphere. Nature 317 (6032), 27–35.

César, A.C.G., Carvalho Jr., J.A., Nascimento, L.F.C., 2015. Association between NOx exposure and deaths caused by respiratory diseases in a medium-sized Brazilian city. Braz. J. Med. Biol. Res. 48, 1130–1135.

CETESB, 2020. Relatório de qualidade do ar CETESB, Relatório de qualidade do ar no estado de São Paulo. São Paulo, Brazil.

Charlson, R.J., Rodhe, H., 1982. Factors controlling the acidity of natural rainwater. Nature 295 (5851), 683–685.

Cheng, I., Zhang, L., 2017. Long-term air concentrations, wet deposition, and scavenging ratios of inorganic ions, HNO3, and SO2 and assessment of aerosol and precipitation acidity at Canadian rural locations. Atmos. Chem. Phys. 17 (7), 4711–4730.

Comly, H.H., 1945. Cyanosis in infants caused by nitrates in well water. J. Am. Med. Assoc. 129 (2), 112–116.

De Mello, W.Z., 2001. Precipitation chemistry in the coast of the metropolitan region of Rio de Janeiro, Brazil. Environ. pollut. 114 (2), 235–242.

de Miranda, R.M., de Fatima Andrade, M., Fornaro, A., Astolfo, R., de Andre, P.A., Saldiva, P., 2012. Urban air pollution: a representative survey of PM2.5 mass concentrations in six Brazilian cities. Air Quality, Atmos. Health. 5 (1), 63–77.

Donahoe, W.E., 1949. Cyanosis in infants with nitrates in drinking water as cause. Pediatrics 3 (3), 308–311.

Elliott, E.M., Kendall, C., Wankel, S.D., Burns, D.A., Boyer, E.W., Harlin, K., Bain, D.J., Butler, T.J., 2007. Nitrogen isotopes as indicators of NO x source contributions to atmospheric nitrate deposition across the midwestern and northeastern United States. Environ. Sci. Technol. 41 (22), 7661–7667.

Elliott, E.M., Yu, Z., Cole, A.S., Coughlin, J.G., 2019. Isotopic advances in understanding reactive nitrogen deposition and atmospheric processing. Sci. Total Environ. 662, 393–403.

Epe, E.D.P.E., 2020. Balanço Energético Nacional 2020: Ano Base 2019. Empresa de Pesquisa Energética.

Fahey, T.J., Williams, C.J., Rooney-Varga, J.N., Cleveland, C.C., Postek, K.M., Smith, S. D., Bouldin, D.R., 1999. Nitrogen deposition in and around an intensive agricultural district in central New York. Am. Soc. Agron. Crop Sci. Soc. Am. Soil Sci. Soc. Am. 28 (5), 1585–1600.

Fang, Y.T., Koba, K., Wang, X.M., Wen, D.Z., Li, J., Takebayashi, Y., Liu, X.Y., Yoh, M., 2011. Anthropogenic imprints on nitrogen and oxygen isotopic composition of precipitation nitrate in a nitrogen-polluted city in southern China. Atmos. Chem. Phys. 11 (3), 1313–1325.

FAOSTAT, 2018. FAOSTAT Statistical Database [WWW Document]. Food Agric. Organ. United Nations (FAO), Rome. URL. http://www.fao.org/faostat/en/#compare, 8.12.21.

FEAM - Fundação Estadual de Meio Ambiente de Minas Gerais, 2022. Monitoramento da Qualidade do Ar na Região Metropolitana de Belo Horizonte, 2015-2021. URL. http://www.feam.br/component/content/article/15/1753-belo-horizonte, 06.14.22.

Felix, J.D., Murgulet, D., 2020. Nitrate isotopic composition of sequential Hurricane Harvey wet deposition: low latitude NOx sources and oxidation chemistry. Atmos. Environ. 238, 117748.

Fieberg, J., 2007. Kernel density estimators of home range: smoothing and the autocorrelation red herring. Ecology 88 (4), 1059–1066.

Fowler, D., Pyle, J.A., Raven, J.A., Sutton, M.A., 2013. The global nitrogen cycle in the twenty-first century: introduction. Phil. Trans. Biol. Sci. 368 (1621), 20130165.

Freyer, H.D., 1991. Seasonal variation of 15N/14N ratios in atmospheric nitrate species. Tellus B 43 (1), 30–44.

Freyer, H.D., Kley, D., Volz-Thomas, A., Kobel, K., 1993. On the interaction of isotopic exchange processes with photochemical reactions in atmospheric oxides of nitrogen. J. Geophys. Res. Atmos. 98 (D8), 14791–14796.

Fu, Y., Wang, W., Han, M., Kuerban, M., Wang, C., Liu, X., 2019. Atmospheric dry and bulk nitrogen deposition to forest environment in the North China Plain. Atmos. Pollut. Res. 10 (5), 1636–1642.

Gaffney, J.S., Marley, N.A., 2009. The impacts of combustion emissions on air quality and climate–From coal to biofuels and beyond. Atmos. Environ. 43 (1), 23–36.

Galloway, J.N., Dentener, F.J., Capone, D.G., Boyer, E.W., Howarth, R.W., Seitzinger, S. P., Asner, G.P., Cleveland, C.C., Green, P.A., Holland, E.A., Karl, D.M., Michaels, A. F., Porter, J.H., Townsend, A.R., Vöosmarty, C.J., 2004. Nitrogen cycles: past,

present, and future. Biogeochemistry 70, 153–226. https://doi.org/10.1007/s10533-004-0370-0.
Galloway, J.N., Likens, G.E., Keene, W.C., Miller, J.M., 1982. The composition of precipitation in remote areas of the world. J. Geophys. Res.: Oceans 87 (C11), 8771–8786.
Galloway, J.N., Townsend, A.R., Erisman, J.W., Bekunda, M., Cai, Z., Freney, J.R., Martinelli, L.A., Seitzinger, S.P., Sutton, M.A., 2008. Transformation of the nitrogen cycle: recent trends, questions, and potential solutions. Science 320 (5878), 889–892. https://doi.org/10.1126/science.1136674.
Gouveia, N., Leon, A.P.D., Junger, W., Lins, J.D.F., Freitas, C.U.D., 2019. Poluição do ar e impactos na saúde na Região Metropolitana de Belo Horizonte–Minas Gerais, Brasil, vol. 24. Ciência & Saúde Coletiva, pp. 3773–3781.
Hastings, M.G., Sigman, D.M., Lipschultz, F., 2003. Isotopic evidence for source changes of nitrate in rain at Bermuda. J. Geophys. Res. Atmos. 108 (D24).
Hastings, M.G., Steig, E.J., Sigman, D.M., 2004. Seasonal variations in N and O isotopes of nitrate in snow at Summit, Greenland: implications for the study of nitrate in snow and ice cores. J. Geophys. Res. Atmos. 109 (D20).
Heaton, T.H.E., 1990. 15N/14N ratios of NOx from vehicle engines and coal-fired power stations. Tellus B 42 (3), 304–307.
Hoinaski, L., Franco, D., Haas, R., Martins, R.F., Lisboa, H.D.M., 2014. Investigation of rainwater contamination sources in the southern part of Brazil. Environ. Technol. 35 (7), 868–881.
Jia, G., Chen, F., 2010. Monthly variations in nitrogen isotopes of ammonium and nitrate in wet deposition at Guangzhou, south China. Atmos. Environ. 44 (19), 2309–2315.
Jiang, X.Q., Mei, X.D., Feng, D., 2016. Air pollution and chronic airway diseases: what should people know and do? J. Thorac. Dis. 8 (1), E31.
Jin, Z., Wang, Y., Qian, L., Hu, Y., Jin, X., Hong, C., Li, F., 2019. Combining chemical components with stable isotopes to determine nitrate sources of precipitation in Hangzhou and Huzhou, SE China. Atmos. Pollut. Res. 10 (2), 386–394.
Junior, O.P., de Almeida Pinto, I.R.C., 2021. Brasil campeão mundial de raios. Artliber.
Karna, A., Gibert, K., 2022. Automatic identification of the number of clusters in hierarchical clustering. Neural Comput. Appl. 34 (1), 119–134.
Kendall, C., Elliott, E.M., Wankel, S.D., 2008. Tracing Anthropogenic Inputs of Nitrogen to Ecosystems, second ed. Blackwell Publishing, Oxford, United Kingdom, pp. 375–449. Stable isotopes in ecology and environmental science.
Kim, E., Hopke, P.K., Edgerton, E.S., 2003. Source identification of Atlanta aerosol by positive matrix factorization. J. Air Waste Manag. Assoc. 53 (6), 731–739.
Krankowsky, D., Bartecki, F., Klees, G.G., Mauersberger, K., Schellenbach, K., Stehr, J., 1995. Measurement of heavy isotope enrichment in tropospheric ozone. Geophys. Res. Lett. 22 (13), 1713–1716.
Li, D., Wang, X., 2008. Nitrogen isotopic signature of soil-released nitric oxide (NO) after fertilizer application. Atmos. Environ. 42 (19), 4747–4754.
Li, Z., Walters, W.W., Hastings, M.G., Zhang, Y., Song, L., Liu, D., Zhang, W., Pan, Y., Fu, P., Fang, Y., 2019. Nitrate isotopic composition in precipitation at a Chinese megacity: seasonal variations, atmospheric processes, and implications for sources. Earth Space Sci. 6 (11), 2200–2213.
Liu, X., Ju, X., Zhang, Y., He, C., Kopsch, J., Fusuo, Z., 2006. Nitrogen deposition in agroecosystems in the Beijing area. Agric. Ecosyst. Environ. 113 (1–4), 370–377.
Liu, X.Y., Xiao, H.W., Xiao, H.Y., Song, W., Sun, X.C., Zheng, X.D., Liu, C.Q., Koba, K., 2017. Stable isotope analyses of precipitation nitrogen sources in Guiyang, southwestern China. Environ. Pollut. 230, 486–494.
Liu, X.Y., Yin, Y.M., Song, W., 2020. Nitrogen isotope differences between major atmospheric NO y species: implications for transformation and deposition processes. Environ. Sci. Technol. Lett. 7 (4), 227–233.
Lucio, P.S., de Toscano, E.M.M., de Abreu, M.L., 1999. Punctual climatic series characteristics, using correspondence analysis. Case study: Belo Horizonte-MG (Brazil). Rev. Bras. Geofís. 17 (2–3), 193–207.
Macêdo, M.F.M., Ramos, A.L.D., 2020. Vehicle atmospheric pollution evaluation using AERMOD model at avenue in a Brazilian capital city. Air Quality, Atmos. Health. 13 (3), 309–320.
Matiatos, I., 2016. Nitrate source identification in groundwater of multiple land-use areas by combining isotopes and multivariate statistical analysis: a case study of Asopos basin (Central Greece). Sci. Total Environ. 541, 802–814.
Matiatos, I., Wassenaar, L.I., Monteiro, L.R., Terzer-Wassmuth, S., Douence, C., 2022. Isotopic composition (δ15N, δ18O) of nitrate in high-frequency precipitation events differentiate atmospheric processes and anthropogenic NOx emissions. Atmos. Res. 267, 105971.
Matiatos, I., Wassenaar, L.I., Monteiro, L.R., Venkiteswaran, J.J., Gooddy, D.C., Boeckx, P., Sacchi, E., Yue, F.J., Michalski, G., Alonso-Hernández, C., Biasi, C., 2021. Global patterns of nitrate isotope composition in rivers and adjacent aquifers reveal reactive nitrogen cascading. Commun. Earth Environ. 2 (1), 1–10.
Matthias, V., Bewersdorff, I., Aulinger, A., Quante, M., 2010. The contribution of ship emissions to air pollution in the North Sea regions. Environ. Pollut. 158 (6), 2241–2250.
Monteiro, L.R., Terzer-Wassmuth, S., Matiatos, I., Douence, C., Wassenaar, L.I., 2021. Distinguishing in-cloud and below-cloud short and distal N-sources from high-temporal resolution seasonal nitrate and ammonium deposition in Vienna, Austria. Atmos. Environ. 266, 118740.
Moore, H., 1977. The isotopic composition of ammonia, nitrogen dioxide and nitrate in the atmosphere. Atmos. Environ. 11 (12), 1239–1243.
Morin, S., Savarino, J., Frey, M.M., Domine, F., Jacobi, H.W., Kaleschke, L., Martins, J. M., 2009. Comprehensive isotopic composition of atmospheric nitrate in the Atlantic Ocean boundary layer from 65 S to 79 N. J. Geophys. Res. Atmos. 114 (D5).
Morin, S., Savarino, J., Frey, M.M., Yan, N., Bekki, S., Bottenheim, J.W., Martins, J.M., 2008. Tracing the origin and fate of NOx in the Arctic atmosphere using stable isotopes in nitrate. Science 322 (5902), 730–732.
Ohara, T.A.H.K., Akimoto, H., Kurokawa, J.I., Horii, N., Yamaji, K., Yan, X., Hayasaka, T., 2007. An Asian emission inventory of anthropogenic emission sources for the period 1980–2020. Atmos. Chem. Phys. 7 (16), 4419–4444.
Passos, R.G., Cota, S.D.S., Menezes, M.Â.D.B.C., Palmieri, H.E.L., de Alencar Auler, L.M. L., 2021. Effect of partial lockdown due to Covid-19 pandemic on PM10 concentration in Belo Horizonte, Brazil. Desenvolv. Meio Ambiente 58.
PETROBRAS, 2018. Relatório Técnico - Atualização do Inventário das Fontes de Emissão de Poluentes Atmosféricos da Região de Belo Horizonte, Contagem e Betim. Belo Horizonte, Brazil.
Rose, L.A., Yu, Z., Bain, D.J., Elliott, E.M., 2019. High Resolution, Extreme Isotopic Variability of Precipitation Nitrate, vol. 207. Atmospheric Environment, pp. 63–74.
Samara, C., Tsitouridou, R., Balafoutis, C., 1992. Chemical composition of rain in Thessaloniki, Greece, in relation to meteorological conditions. Atmos. Environ. Part B Urban Atmos. 26 (3), 359–367.
Sant'Anna, A.A., Costa, L., 2021. Environmental regulation and bail outs under weak state capacity: deforestation in the Brazilian Amazon. Ecol. Econ. 186, 107071.
Schumann, U., Huntrieser, H., 2007. The global lightning-induced nitrogen oxides source. Atmos. Chem. Phys. 7 (14), 3823–3907.
Shi, Y., Li, C., Jin, Z., Zhang, Y., Xiao, J., Li, F., 2021. Combining Dual Isotopes and a Bayesian Isotope Mixing Model to Quantify the Nitrate Sources of Precipitation in Ningbo, East China, vol. 778. Science of The Total Environment, 146297.
Song, W., Liu, X.Y., Hu, C.C., Chen, G.Y., Liu, X.J., Walters, W.W., Michalski, G., Liu, C. Q., 2021. Important contributions of non-fossil fuel nitrogen oxides emissions. Nat. Commun. 12 (1), 1–7.
Souza, P.A.D., Mello, W.Z.D., Maldonado, J., Evangelista, H., 2006. Composição química da chuva e aporte atmosférico na Ilha Grande, vol. 29. RJ. Química Nova, pp. 471–476.
Stevens, C.J., Dise, N.B., Mountford, J.O., Gowing, D.J., 2004. Impact of nitrogen deposition on the species richness of grasslands. Science 303 (5665), 1876–1879.
Sutton, M.A., Oenema, O., Erisman, J.W., Leip, A., van Grinsven, H., Winiwarter, W., 2011. Too much of a good thing. Nature 472 (7342), 159–161.
Sweevers, H., Van Grieken, R., 1992. Analytical study of the deterioration of sandstone, marble and granite. Atmos. Environ. Part B - Urban Atmos. 26 (2), 159–163.
Tiwari, S., Chate, D.M., Bisht, D.S., Srivastava, M.K., Padmanabhamurty, B., 2012. Rainwater chemistry in the north Western Himalayan region, India. Atmos. Res. 104, 128–138.
Unece, I., 2004. Manual on methodologies and criteria for modelling and mapping critical loads & levels and air pollution effects, risks and trends. In: Convention on Long-Range Transboundary Air Pollution. United Nations Economic Commission for Europe, International Cooperative Programme. http://www.icpmapping.org.
Vet, R., Artz, R.S., Carou, S., Shaw, M., Ro, C.U., Aas, W., Baker, A., Bowersox, V.C., Dentener, F., Galy-Lacaux, C., Hou, A., 2014. A global assessment of precipitation chemistry and deposition of sulfur, nitrogen, sea salt, base cations, organic acids, acidity and pH, and phosphorus. Atmos. Environ. 93, 3–100.
Villalobos-Forbes, M., Esquivel-Hernández, G., Sánchez-Murillo, R., Sánchez-Gutiérrez, R., Matiatos, I., 2021. Stable isotopic characterization of nitrate wet deposition in the tropical urban atmosphere of Costa Rica. Environ. Sci. Pollut. Control Ser. 28 (47), 67577–67592.
Vystavna, Y., Schmidt, S.I., Kopáček, J., Hejzlar, J., Holko, L., Matiatos, I., Wassenaar, L. I., Persoiu, A., Badaluta, C.A., Huneau, F., 2020. Small-scale chemical and isotopic variability of hydrological pathways in a mountain lake catchment. J. Hydrol. 585, 124834.
Walters, W.W., Goodwin, S.R., Michalski, G., 2015. Nitrogen stable isotope composition (δ15N) of vehicle-emitted NO x. Environ. Sci. Technol. 49 (4), 2278–2285.
Wankel, S.D., Chen, Y., Kendall, C., Post, A.F., Paytan, A., 2010. Sources of aerosol nitrate to the Gulf of Aqaba: evidence from δ15N and δ18O of nitrate and trace metal chemistry. Mar. Chem. 120 (1–4), 90–99.
WMO, 2004. Manual for the GAW Precipitation Chemistry Programme - Guidelines, Data Quality Objectives and Standard Operating Procedures (New York, USA).
World Health Organization, 2017. Don't Pollute My Future! the Impact of the Environment on Children's Health. World Health Organization (No. WHO/FWC/IHE/17.01).
Xie, Y., Xiong, Z., Xing, G., Yan, X., Shi, S., Sun, G., Zhu, Z., 2008. Source of nitrogen in wet deposition to a rice agroecosystem at Tai lake region. Atmos. Environ. 42 (21), 5182–5192.
Xing, M., Liu, W., 2012. Variations in the concentration and isotopic composition of nitrate nitrogen in wet deposition and their relation with meteorological conditions in Xi'an city, Northwest China. Appl. Geochem. 27 (4), 831–840.
Yu, J., Yan, C., Liu, Y., Li, X., Zhou, T., Zheng, M., 2018. Potassium: a tracer for biomass burning in Beijing? Aerosol Air Qual. Res. 18 (9), 2447–2459.
Zhang, F., Chen, Y., Tian, C., Lou, D., Li, J., Zhang, G., Matthias, V., 2016. Emission factors for gaseous and particulate pollutants from offshore diesel engine vessels in China. Atmos. Chem. Phys. 16 (10), 6319–6334.
Zhang, Y., Liu, X.J., Fangmeier, A., Goulding, K.T.W., Zhang, F.S., 2008. Nitrogen inputs and isotopes in precipitation in the North China Plain. Atmos. Environ. 42 (7), 1436–1448.
Zhao, X., Yan, X., Xiong, Z., Xie, Y., Xing, G., Shi, S., Zhu, Z., 2009. Spatial and temporal variation of inorganic nitrogen wet deposition to the Yangtze River Delta Region, China. Water Air Soil Pollut. 203 (1), 277–289.
Zong, Z., Tian, C., Li, J., Syed, J.H., Zhang, W., Fang, Y., Jiang, Y., Nasir, J., Mansha, M., Rizvi, S.H.H., Shafiq, M., 2020. Isotopic interpretation of particulate nitrate in the metropolitan city of Karachi, Pakistan: insight into the oceanic contribution to NOx. Environ. Sci. Technol. 54 (13), 7787–7797.